Planetary Nebulae: A Universal Toolbox in the Era of Precision Astrophysics
Proceedings IAU Symposium No. 384, 2025
O. De Marco, A. Zijlstra & R. Szczerba, eds.
doi:10.1017/S1743921323005446

A statistical view of low-ionization structures in planetary nebulae

M. Belén Mari[1], Stavros Akras[2] and Denise R. Gonçalves[1]

[1]Valongo Observatory, Federal University of Rio de Janeiro, Rio de Janeiro, Brazil
email: mbmari@unc.edu.ar

[2]Institute for Astronomy, Astrophysics, Space Applications and Remote Sensing, National Observatory of Athens, Greece

Abstract. More than three decades after the pioneering imaging catalog by Balick (1987), where the small-scale and low-ionization structures (LISs) in planetary nebulae (PNe) became evident, the present study conducts a comprehensive statistical analysis of LISs' physical-chemical and excitation properties. Gathering the largest dataset to date, we compare LISs with high-ionization components (rims/shells) across a diverse sample of PNe. Key findings include lower electron densities (N_e[S II]) in LISs than in adjacent rims/shells and comparable electron temperatures (T_e [N II] and [O III]) between these two nebular componets. Various optical diagnostic diagrams, while revealing a clear excitation stratification between these groups of components, are not good enough to clearly pinpoint the main excitation mechanism behind the LISs line-emission. Photoionization and shock models highlight a notable overlap between mechanisms, emphasizing the coexistence of both excitation processes. Contrary to expectations, shocks are unlikely to be the primary excitation source for most of LISs in PNe.

Keywords. ISM: jets and outflows; ISM; kinematics and dynamics; planetary nebulae: general

1. Introduction

Planetary nebulae (PNe) exhibit a variety of morphologies, which are based on the shape of the large-scale, high-ionization) structures such as rims, shells or haloes. In addition, PNe possess small-scale structures prominent in low-ionization species, such as [N II], [S II], [O II] and also [O I]. Gonçalves et al. (2001) classified these low-ionization structures (LISs) considering not only the morphology but also the kinematics, into four main groups: knots, which can appear isolated or in pairs, displaying an aspect ratio close to 1; filaments, when this aspect ratio mentioned before is larger than 1; jets, which appear in opposite pairs, oriented in radial direction from the central star (CS) and have velocities notably higher than the surrounding gas; and jet-like structures, when the velocity of these jets is similar to that of the large-scale structures on which the LISs are embedded. Note that this term, *LISs*, encompasses a broader category that includes various structures falling under this classification, which, in the literature, may also be referred to by more specific nomenclatures: fast low-ionization emission regions (FLIERs) by Balick et al. (1993), bipolar rotating episodic jets (BRETs) by Lopez et al. (1995) or slow moving low-ionization emission regions (SLOWERs) by Perinotto (2000).

Many authors have tried to understand the LISs' properties through, in particular, optical spectra (e.g. Balick et al. 1993, 1994; Gonçalves et al. 2003, 2009; Akras & Gonçalves 2016; Mari et al. 2023a). The conclusions arrived so far are: (i) LISs appear in all morphological type of PNe; (ii) the electron temperature (T_e) between LISs and the larger structures is almost the same; (iii) the electron density (N_e), in general, is lower in LISs

© The Author(s), 2025. Published by Cambridge University Press on behalf of International Astronomical Union.

https://doi.org/10.1017/S1743921323005446 Published online by Cambridge University Press

than in the surrounding medium; and (iv) there is no significant difference in the chemical abundance between LISs and their surrounding medium. Regarding the excitation mechanisms, there is no consensus yet, LISs could be excited by photoionization from the CS (e.g. Hajian et al. 1997; Ali & Dopita 2017), by shocks interactions (Gonçalves et al. 2004) or by both mechanisms (Fang et al. 2015; Akras & Gonçalves 2016).

In an effort to gain deeper insights into the characteristics of LISs, we initiated a comprehensive study by compiling optical properties obtained from published research over the years. Similar to Guerrero et al. (2020), where efforts were made to enhance the understanding of kinematic properties of LISs within PNe, our objective here is to attain robust and reliable results concerning physico-chemical properties. Section 2 provides an overview of the data we have gathered and our approach to visualizing it. In Section 3, we present the key findings, while Section 4 highlights the discuss and main conclusions arrived.

2. Collected data and visualization

Considering optical spectroscopic studies aimed at understanding LISs within PNe published over the years (e.g. Balick et al. 1994; Hajian et al. 1997; Gonçalves et al. 2003; Fang et al. 2015; Akras & Gonçalves 2016; Ali & Dopita 2017; Miranda et al. 2021; Mari et al. 2023a) we have compiled a dataset of 33 PNe, encompassing 88 rims/shells and 104 LISs. Our choice was to conduct a statistical analysis, employing violinplots – a hybrid visualization method that combines elements of both boxplots and kernel density distributions. One of the most important quantities, in addition to the quartiles and the median, which represents the most expected value, pertains to the *notches*. They serve as boundaries for the 95% confidence interval (CI) of the median value within the analyzed data group (Hintze & Nelson 1998). With the objective of contrasting the features of rims/shells and LISs to discern potential similarities or differences, notches emerge as a valuable analytical tool. Non-overlapping confidence intervals (CIs) imply statistical dissimilarity between groups, while overlapping CIs suggest similarity in the specified property (Chambers & et al. 2017).

3. Results

This section compiles the primary results obtained through the utilization of violin plots.

3.1. *Electron density*

Upon the examination of electron density based on sulfur diagnostic lines (N_e[S II]), in Fig. 1 it can be observed two distinct distributions: one represented in green denoting the LISs distribution, and the other in cyan, signifying the rims/shells distribution. A split violinplot analysis revealed non-overlapping CIs for both distributions, corroborated by the statistical values in Table 1. Consequently, it can be deduced that the two groups exhibit statistically significant differences with respect to N_e[S II]. Further accentuating the contrasting N_e[S II] between the two distinct nebular components is illustrated in the right panel of Fig. 1. This panel directly compares the median N_e[S II] per PN for rims/shells and LISs. This analysis leads to the same unequivocal inference that the electron densities of LISs are notably lower than those of rims/shells.

3.2. *Electron temperature*

In terms of electron temperature (T_e) derived from the [N II] diagnostic lines, the analysis indicates an overlap in the CIs, as presented in Table 1. This result is further

https://doi.org/10.1017/S1743921323005446 Published online by Cambridge University Press

Table 1. N_e (in particles per cm^{-3}) and T_e (in K) for the samples of rims/shells and LISs. The CI correspond to the approximated 95 per cent of confidence intervals for the median value. The last two rows show the number of outliers and sample size, respectively.

	log(N_e[S II])		log(T_e[N II])		log(T_e[O III])	
	Rims/Shells	LISs	Rims/Shells	LISs	Rims/Shells	LISs
Median	3.42	3.23	4.03	4.04	4.01	4.06
CI	[3.35;3.50]	[3.15;3.31]	[4.01;4.05]	[4.02;4.06]	[3.98;4.03]	[4.05;4.08]
#Outliers	4	3	2	2	0	3
#Sample	79	98	64	81	79	83

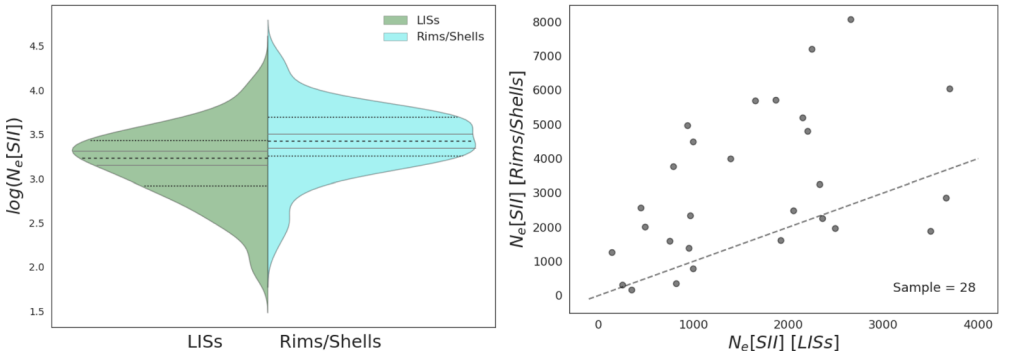


Figure 1. Comparison of N_e[S II] between LISs and rims/shells groups. *Left panel*: split violinplot of both groups with the median, 25th and 75th quartiles shown by dashed and dotted lines, respectively, and the CIs represented by solid lines. *Right panel*: median N_e[S II] values per PN for each group. The dashed line represents the identity function.

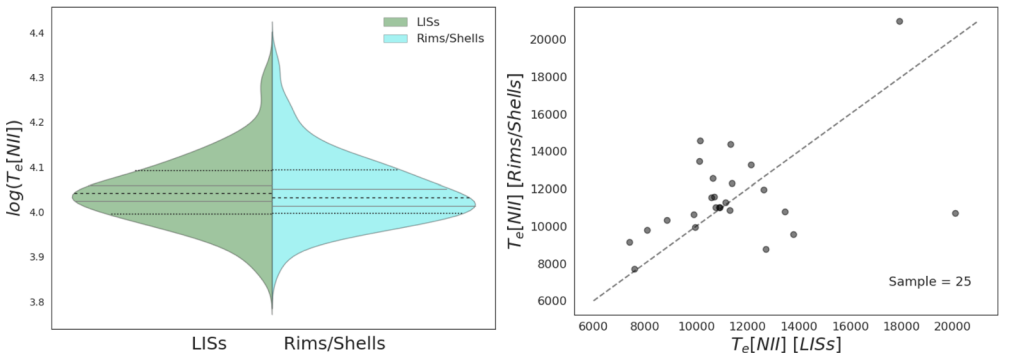


Figure 2. Same as Fig. 1, for T_e[N II].

supported by the similarity observed in the distributions, illustrated in Fig. 2. Therefore, a reasonable conclusion can be drawn that the two groups exhibit a considerable degree of similarity in terms of this electron temperature (T_e[NII]).

When examining the T_e via the [O III] lines, an unexpected bimodality is revealed in the rims/shells group (see Fig. 3), accompanied by non-overlapping CIs (see Table 1). This unanticipated result yields a T_e for LISs that is approximately 1400 K higher than that of rims/shells. Nevertheless, scrutinizing the median values within each group per nebula exposes a dispersion of roughly ±2000 K for both T_e measurements, whether derived from [N II] or [O III] diagnostic lines. Moreover, the right panel of Fig. 3 illustrates minimal discrepancies in median values among the groups within each nebula. In light of this, it can be concluded that the 1400 K difference between the groups falls well within the scatter and does not carry statistical significance. Hence, the datasets indicate comparability in T_e measurements, even when using the [O III] lines.

https://doi.org/10.1017/S1743921323005446 Published online by Cambridge University Press

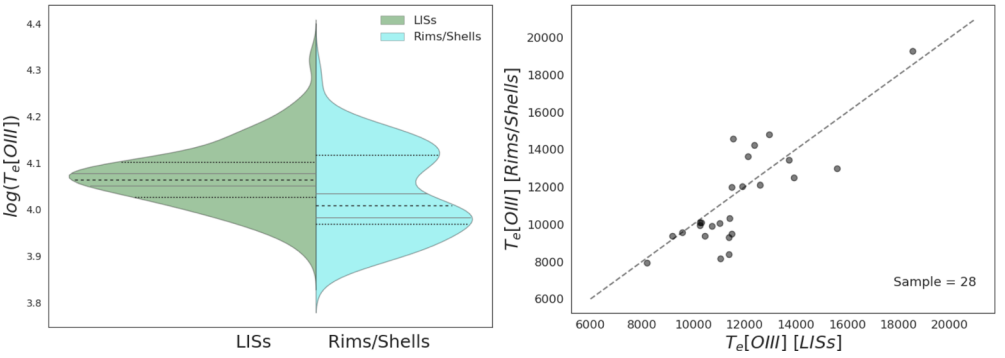


Figure 3. Same as Fig. 1, for T_e[O III].

3.3. *Excitation mechanisms*

In our exploration of excitation mechanisms, we have employed various diagnostic diagrams (DDs), such as those of Sabbadin, Minello & Bianchini (1977) (SMB) and Baldwin, Phillips & Terlevich (1981) (BPT), to distinguish between different objects like H II regions, supernova remnants (SNR) or PNe. SMB relies on Hα/[S II] and Hα/[N II] line ratios to separate these objects. On the other hand, BPT diagrams utilize the [O III]/Hβ line ratio in addition to low-ionization lines over Hα. In our analysis, we employed these DDs to discern excitation mechanisms among the distinct components within the analyzed PNe. As illustrated in Fig. 4, the line ratios involving low-ionization lines do not show overlap in terms of CIs between the groups, which can be interpreted as distinct states of excitation among the analyzed components. In the case of the ratios involving [O III], there are overlapping CIs.

To mitigate potential effects from differences in elemental abundances, we have introduced a new DD centered on a single chemical element, specifically oxygen (Fig. 5). Our analysis of split violinplots for [O I]/Hα and [O II]/[O III] reveals distinct separation, with non-overlapping CIs indicating a clear differentiation between the groups – although with a transition region with both groups mixed, evident on the scatter plot. Nevertheless, it is worth noting that the detection of [O I] is not always feasible, resulting in a smaller sample size that requires cautious interpretation of the results.

3.4. *Photoionization and shocks models*

Examining Figs. 4 and 5, it becomes evident that even though LISs and rims/shells fall into statistically distinct groups concerning excitation state, both appear to be associated with regions excited purely by photoionization except for a few structures that fall near the SNR region – i.e., shocks may be the responsible for the excitation of these structures. A grid of photoionization and shock models from the 3MdB (Morisset et al. 2015; Alarie & Morisset 2019) were used in order to look for the range of various emission lines produced by these two mechanisms. Using these models, we applied the same DDs mentioned in the previous section, delineating regions for data corresponding to pure photoionization, as well as low- and high-velocity shock regions.

A substantial overlap between both excitation mechanisms, encompassing not only low-velocity shock models but also those associated with higher velocities, was found. Nonetheless, by employing DDs that take into account the low-ionization line ratios [N II]/[S II] (see left panel of Fig. 6), we managed to differentiate high-velocity shock regions from the region defined by low-velocity shocks, both of which still overlap with the region primarily dominated by photoionization. Furthermore, when

https://doi.org/10.1017/S1743921323005446 Published online by Cambridge University Press

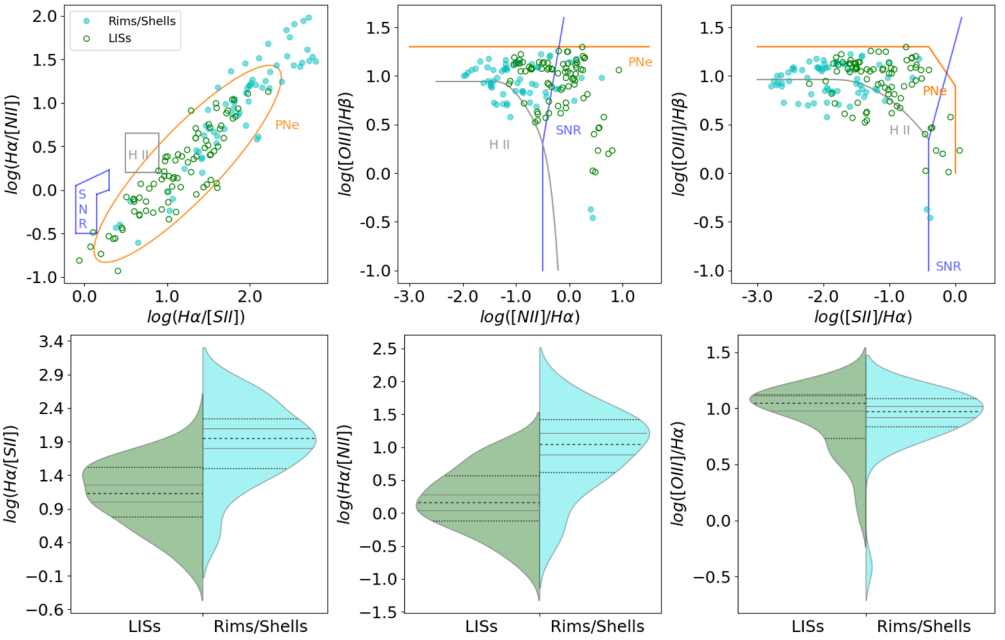


Figure 4. Diagnostic diagrams employed in this work (upper panels) and the split violinplots of their ratio lines (lower panels).

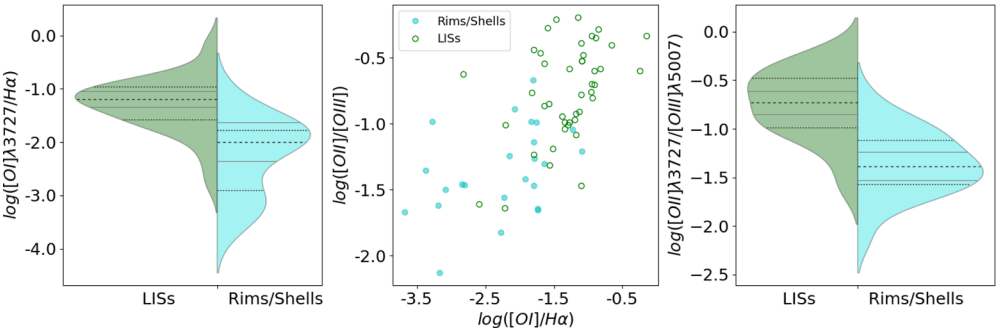


Figure 5. Diagnostic diagram depending on oxygen (middle panel), together with its split violinplots.

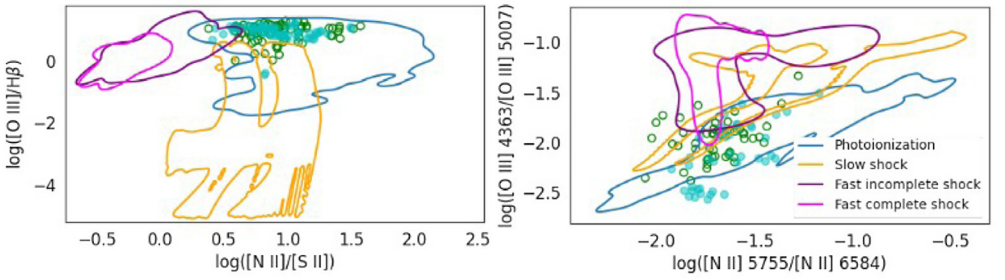


Figure 6. Diagnostic diagrams generated from grids of photoionization and shocks models available in the 3MdB. The photoionization models are in blue contour, the low- and high-velocity shock models are in orange and purple contours, respectively. Our sample of LISs and rims/shells are shown with unfilled green circles and filled cyan circles as before.

https://doi.org/10.1017/S1743921323005446 Published online by Cambridge University Press

utilizing temperature-sensitive line ratios, specifically [N II]λ5755/[N II]λ6584 versus [O III]λ4363/[O III]λ5007 (right panel of Fig. 6), we can distinguish high- and low-velocity shock regions from the location of the objects predominantly excited by photoionization (Mari et al. 2023b).

4. Discussion and conclusions

Returning to the contrast observed in electron density (N_e) between the two groups, a follow-up investigation involving the median values of each group per nebula confirmed that the N_e for rims/shells is indeed higher than that for LISs, with measured median value around 1700 cm^{-3}. Notably, this result appear contradictory to models predicting higher total densities for observed knots (Raga et al. 2008) in comparison with their surrounding gas, or more recently for knots at the tip of the jets having total density in the range of 10^6 to 10^7 cm^{-3}, coupled with low temperatures in the range of 1 to 300 K (Balick et al. 2020). In an effort to address this discrepancy, Gonçalves et al. (2009) proposed the possibility that a substantial fraction of the gas may exist in a neutral or molecular state, which is supported by the limited number of LISs in PNe with the detection of H_2 in the near-IR (Fang et al. 2015, 2018; Akras et al. 2017, 2020). Nonetheless, additional investigations are required to explore new results in the near-IR by examining H_2 and, similarly, in the millimeter range to search for CO, the two most abundant molecules in the universe.

Therefore, considering that this study utilized the most extensive sample of LISs to date and employed statistical analysis, the overall conclusions are more robust. The key findings are as follows: (i) There is no significant difference between the two groups in terms of T_e when using either [N II] or [O III] diagnostic lines. (ii) LISs do indeed exhibit lower electron density compared to the surrounding gas, reinforcing the hypothesis of the presence of neutral and/or molecular matter in their interiors. (iii) Using classical diagnostic diagrams, it is evident that the separation between the groups demonstrates an excitation stratification within PNe, meaning two distinct groups in terms of excitation. However, the majority of LISs are primarily excited by photoionization, with only a few potentially influenced by shocks. (iv) The utilization of multiple DDs may provide a more reliable method of distinguishing between different excitation mechanisms.

Acknowledgements. We acknowledge the partial support: MBM (Capes; IAU and FAPERJ/200.527/2023); DRG (CNPq313016/2020-8 and FAPERJ/200.527/2023); SA (H.F.R.I. Project Number: 15665).

References

Akras S., Gonçalves D. R., 2016, MNRAS, 455, 930
Akras S., Gonçalves D. R., Ramos-Larios G., 2017, MNRAS, 465, 1289
Akras S., Gonçalves D. R., Ramos-Larios G., Aleman I., 2020, MNRAS, 493, 3800
Alarie A., Morisset C., 2019, RMxAA, 55, 377
Ali A., Dopita M. A., 2017, PASA, 34, e036
Baldwin J. A., Phillips M. M., Terlevich R., 1981, PASP, 93, 5
Balick B., Rugers M., Terzian Y., Chengalur J. N., 1993, ApJ, 411, 778
Balick B., Perinotto M., Maccioni A., Terzian Y., Hajian A., 1994, ApJ, 424, 800
Balick B., Frank A., Liu B., 2020, ApJ, 889, 13
Chambers J. M., et al. 2017, Graphical Methods for Data Analysis. 1st Ed., doi:10.1201/9781351072304
Fang X., Guerrero M. A., Miranda L. F., Riera A., Velázquez P. F., Raga A. C., 2015, MNRAS, 452, 2445
Fang X., Zhang Y., Kwok S., Hsia C.-H., Chau W., Ramos-Larios G., Guerrero M. A., 2018, ApJ, 859, 92

https://doi.org/10.1017/S1743921323005446 Published online by Cambridge University Press

Gonçalves D. R., Corradi R. L. M., Mampaso A., 2001, ApJ, 547, 302
Gonçalves D. R., Corradi R. L. M., Mampaso A., Perinotto M., 2003, ApJ, 597, 975
Gonçalves D. R., Mampaso A., Corradi R. L. M., Perinotto M., et al. 2004, MNRAS, 355, 37
Gonçalves D. R., Mampaso A., Corradi R. L. M., Quireza C., 2009, MNRAS, 398, 2166
Guerrero M. A., Suzett Rechy-García J., Ortiz R., 2020, ApJ, 890, 50
Hajian A. R., Balick B., Terzian Y., Perinotto M., 1997, ApJ, 487, 304
Hintze J. L., Nelson R. D., 1998, The American Statistician, 52, 181
Lopez J. A., Vazquez R., Rodriguez L. F., 1995, Astrophys. J. Let., 455, L63
Mari M. B., Gonçalves D. R., Akras S., 2023a, MNRAS, 518, 3908
Mari M. B., Akras S., Gonçalves D. R., 2023b, MNRAS, 525, 1998
Miranda L. F., et al., 2021, arXiv e-prints, p. arXiv:2105.05186
Morisset C., Delgado-Inglada G., Flores-Fajardo N., 2015, RMxAA, 51, 103
Perinotto M., 2000, Astrophys. Space Sci., 274, 205
Raga A. C., Riera A., Mellema G., Esquivel A., Velázquez P. F., 2008, A&A, 489, 1141
Sabbadin F., Minello S., Bianchini A., 1977, A&A, 60, 147

https://doi.org/10.1017/S1743921323005446 Published online by Cambridge University Press